Bulgarian Academy of Sciences. Space Research and Technology Institute.
Aerospace Research in Bulgaria. 31, 2019, Sofia

DOI: https://doi.org/10.3897/arb.v31.e04

THE GLOBAL TEMPERATURE ANOMALIES RELATED TO THE SLOWDOWN OF ATMOSPHERIC CO2 CONCENTRATION OBSERVED FROM 1939 UP TO 1950

Rolf Werner, Veneta Guineva

Space Research and Technology Institute – Bulgarian Academy of Sciences
e-mail: rolwer52@yahoo.co.uk

Keywords: *Global temperatures, Atmosphere, Temperature anomalies, CO_2.*

Abstract

It is very well known that carbon dioxide (CO_2) accumulated in the atmosphere is the main climate driver. The first precise direct continuous measurements of the atmospheric CO_2 concentration were provided from Keeling since 1958 at Mauna Loa Observatory. The measurements are going on up to day. Law Dom ice core drilling was started in 1969 by the Australian ANARE program.

The slowdown of the World economic development during the World War I, the Great Depression and the World War II lead to a deceleration of the CO_2 emissions. The integration of the total CO_2 emissions using the impulse response function concept shows that the observed slowdown of the CO_2 emission is not sufficient to explain the CO_2 plateau and additional CO_2 sinks are necessary. Based on multiple regression models adjusted global temperatures were determined by removal of temperature influences other than related to CO_2. The adjusted temperatures follow close the CO_2 radiation term. The difference between the estimated adjusted temperature time evolution with and without the CO_2 slowdown and also the short time trends demonstrate very clear the close relation between the temperature change and the CO_2 radiative forcing. It is shown that the slowdown of the CO_2 emission in the period from 1939 to 1950 and the related CO_2 concentration in the atmosphere, caused at least partially by human activities, generate slower increase of the temperature anomalies. Consequently CO_2 is the leading variable of the relation surface temperature – CO_2.

Introduction

Global warming is usually perceived as the increase of the average global temperature over a long period of time, usually 30 years or more. The global temperatures inferred from direct observations show a rise of approximately 0.7 °C during the 20th century. The temperatures however do not increase continuously. Longer periods of warming alternate with periods in which the temperature does not increase or a cooling is observed. The global temperature series are characterized also by variations on the scale from decades to years associated with El Niño events, with volcano eruptions and with changes in the solar activity. Lean and Rind [1] explained 76% of the temperature variance by indices describing anthropogenic forcing, El Niño/ Southern Oscillation (ENSO) events, volcano activity and solar irradiance changes using multiple regression method analysing the monthly combined land and ocean surface temperature series (HadCRUT3 vcgl) for the period 1889–2006. Foster and Rahmstorf [2] have performed multiple regressions of five different temperature series for the time span of 1979–2010. They have constructed adjusted data sets by removal of the influence of ENSO, volcanic eruptions and the total solar irradiance on the temperatures. They stated that the trends of the adjusted series were linear after 1998 when the greenhouse gases concentrations increased as before, but the rise of the global temperatures seems to be slower in comparison with the period before. It is well known that the oceans are thermally inert and provide an important memory of the climate variations. The inter-decadal Pacific oscillation signal has quasiperiodic variations of the time scale of 15–30 years and is connected to other teleconnections.

The Atlantic multi-decadal oscillation (AMO) was detected by Schlesinger and Ramankutty [3]. It is defined by the Sea surface temperature (SST) anomaly pattern in the Northern Atlantic, where the global warming influence was removed using different methods (see [4] for more details). The AMO shows a periodicity of approximately 65–70 years. The reasons of AMO multi-decadal periodicities are not fully understood until now and they are discussed controversially. Some authors state that the origin of AMO is an intrinsic mode in the dynamic of the ocean-atmosphere system without external forces. It is shown that AMO is driven by the Atlantic meridional overturning circulation [5]. Knudsen et al. [6] explicitly reject the hypothesis that AMO was forced by changes in the solar activity. Other authors found a link with the solar activity long-term changes at multidecadal scales, e.g. [7]. Different studies have demonstrated relations between regional weather phenomena and AMO ([8] and the citations herein). Rohde et al. [9] found an AMO signal in the residuals of the Berkeley Earth global land temperature series modelled by the logarithm of the CO_2 concentration and by volcanic sulphate emissions. For the first time Zhou and Tung [10] included the AMO index in a multiple regression model as a predictor and determined the global warming rate.

In the science community a wide consensus consists about the origin of the climate change by the increase of the man-made CO_2 emission in the atmosphere. The emitted CO_2 passes into the global carbon cycle, where about 45% of it remains in the atmosphere [11]. The remaining in the atmosphere CO_2 absorbs the long-wave radiation coming from the Earth surface. One part of the absorbed radiation is trapped as heat in the atmosphere and another part is re-emitted in all directions, downwards and upwards. This process is the basic understanding of the warming by greenhouse gases. Up to now there is not an exact proof of the real causes of the climate change by greenhouse gases. In the IPCC reports the term "evidence substantiated by simple physical models" was used. The probability of the man-made individual climate change elements is evaluated by climate experts. The evidence of man-made origin of the climate change is demonstrated also by certain patterns in the spatial, temporal or spatial-temporal domain, obtained by climate models and confirmed by observations. One of the most known patterns (or so called finger prints) is e.g. the increase of the temperature in the lower troposphere and the simultaneous decrease of the temperature in the stratosphere caused by CO_2 taking into account solar, volcanic and ozone temperature effects as well [12]. Another example is the substantial rising of the occurrence of the number of warm days per decade during the period 1951–2003. Simultaneously a slight decrease of the number of cold days and of the diurnal temperature range was observed meaning that the atmosphere warming is faster during the day. This fingerprint was found both by climate model simulations and by investigations of the experimental climate observations [13, 14]. The isotope signature of ^{13}C and ^{14}C in the atmosphere is changing (Suess ^{14}C and ^{13}C effect). ^{14}C isotope content in the atmosphere comes by galactic cosmic rays. The ^{14}C isotope has a decay time of more than 5 700 years. Therefor fossils do not contain ^{14}C. By the CO_2 release in the atmosphere due to fuel combustion the amount of ^{14}C decreases. The ^{13}C isotope concentration is reduced compared to the ^{12}C isotope atmospheric concentration, because millions of years ago fuel was formed by plants, accumulating more of the lighter ^{12}C isotope than of the heavier isotope ^{13}C. This change of the carbon isotopes composition in the atmosphere is a fingerprint of the human activity.

The main goal of this paper is to present a new evidence about the causality between the growing of the atmospheric CO_2 concentration and the temperature increase with the leading role of CO_2.

CO_2 emissions and concentration in the Earth atmosphere

The CO_2 concentration in the Earth atmosphere before the industrial revolution, during the Holocene was almost constant. With the beginning of the industrial revolution after the discovery of the first commercial steam-engines the CO_2 emissions were increasing slowly with the developing of the world economy. The CO_2 amount in the atmosphere is determined by a complicated global balance of the CO_2 exchange between the ocean, biosphere, atmosphere and lithosphere, involving diffusion, advection and dissolving processes. Simple empirical models approximate the carbon concentration as a sum of exponentially decaying pulse response functions, where the time decays are of the order of one up to some hundred years [15]. The global total emissions of CO_2 since 1850 are presented in Fig. 1. The global emissions of CO_2 up to about 1910 were dominated by changes in land use [16]. However the increase of the annual global CO_2 emissions is determined basically by the global emitted CO_2 from fuel combustion, as shown in Fig. 1. The exponential increase of the CO_2 emissions during the industrial revolution is interrupted by a period characterised by a slowdown of the emissions throughout the World Wars I and II (WWI and WWII) and the Great Depression [17, 18]. During this time the global annual land use CO_2 emissions are nearly unchanged at the level between 0.8 and 0.9 GtC/yr (see Fig. 4).

After the WWII the national economies rapidly restored and a boom of the worldwide economic development was registered. Sometimes this period is called Great Acceleration. The rapid economic growth was interrupted by the first and later by the second oil shocks. These economic developments are connected to the corresponding energy consumption and reflect in the CO_2 emissions (see Fig. 1).

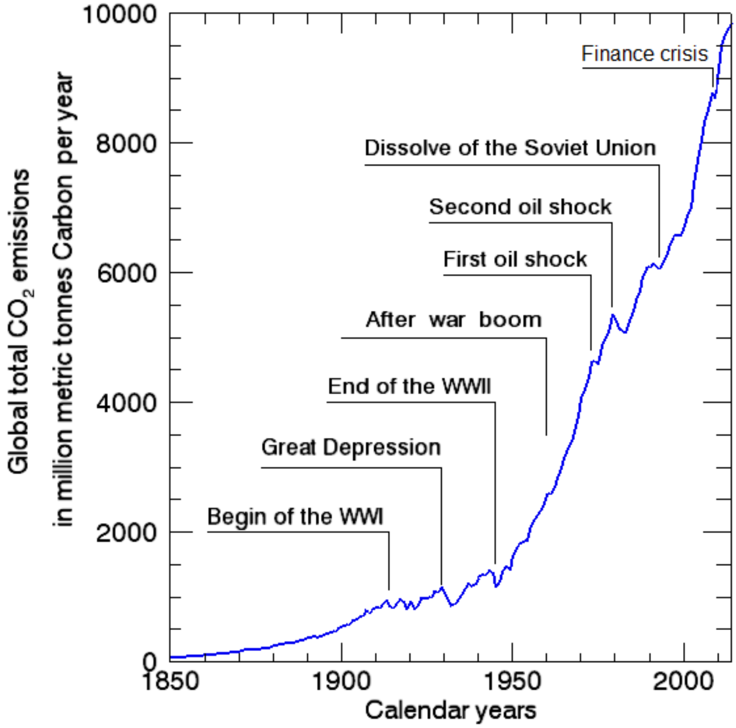

Fig. 1. Total CO_2 emissions including burning of fossil fuel and cement production at the globale scale. The figure is drawn based on the Carbon Dioxide Information Analysis Center (CDIAC) data (http://cdiac.ornl.gov/trends/emis/tre_glob_2013.html) and was redrawn from: http://wiki.bildungsserver.de/klimawandel/index.php/ Datei:FossileEnergie1850–2007.jpg#file.

The concentration of CO_2 accumulated in the atmosphere shows not or only slow increase after 1939 and doesn't achieve the value of 1939 until 1950 as is seen in the CO_2 data compilation from Hansen (http://www.climateaudit.info/ data/hansen/giss_ghg.2007.dat, see also [19]).

MacFarling Meure et al. [20] stated that the CO_2 stabilization between 1940 and 1950 is a notable feature of the ice core measurements and it was verified by newer high density measurements. They confirm this stabilization at 310–312 ppm between 1940 and 1955 (see Fig. 1 in the previously cited paper [20]). For comparison in Fig. 2 the atmospheric CO_2 concentration obtained by different methods throughout different campaigns is presented. Indirect determination of atmospheric CO_2 by analysing air bubbles trapped in polar ice at the Low Dom station in the East Antarctic as well as direct atmospheric CO_2 observations at Mauna Loa beginning in 1958 and at Cape Grim (Tasmania, Australia) from 1978 up to 2015 are included (see also [21]). The uncertainties of the ice core measurements are 1.2 ppm [22].

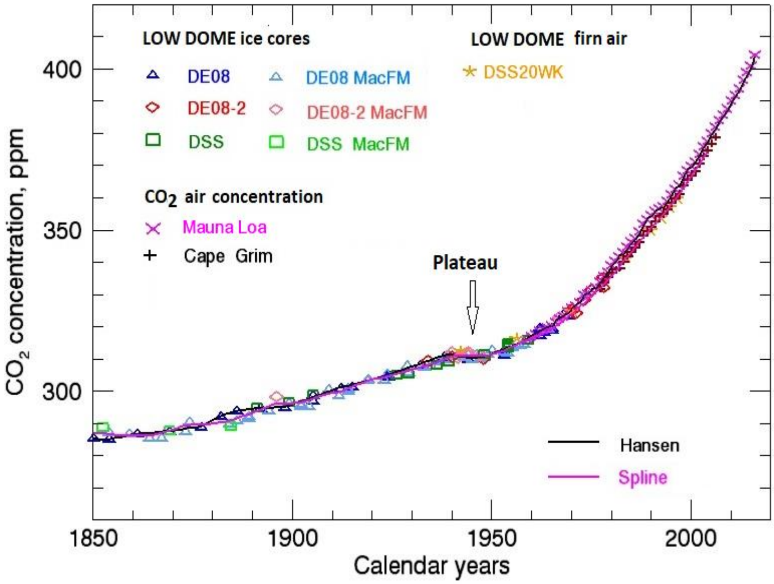

Fig. 2. Increase of the CO_2 concentration in the Earth's atmosphere established by indirect measurements in ice cores DE08, DE08-2 and DSS at the Antarctic station Low Dom since 1850 and established annual means of the CO_2 concentration by direct measurements at Mauna Loa and at Cape Grim, where the CDIAC data and data of the CSIRO Marine and Atmospheric Research and the Australian Bureau of Meteorology were used. The continuous black line is the data compilation of [19], which was extended by means of regression up to 2016. The continuous line in magenta presents a spline attenuate variations with periods of < 20 years by 50% as given by [19], based on [22].

The direct CO_2 concentration measurements are much more accurate and with uncertainties better than 0.2 ppm. (https://www.esrl.noaa.gov/gmd/ccgg/aboutco2_measurements.pdf).

The ice core measurements are smoothed (e.g. by about 10 years for the DE08 core) due to diffusion processes filtering out short term atmospheric CO_2 variations. The atmospheric measurements at Cape Grim show slightly smaller CO_2 concentrations in comparison to the Mauna Loa results, due to the geographical locations – Cape Grim at 40°38' S and Mauna Loa observatory at 19°28' N. The CO_2 concentrations observed at Mauna Loa observatory are closer to the global mean CO_2 amounts in the atmosphere. Therefore these data and the extended by linear regression Hansen's data compilation are used in this paper.

The remaining in the atmosphere amount of CO_2 is given by the imbalance between the CO_2 sources and sinks. The CO_2 sources are the total CO_2 emission consisting mainly from the fuel combustion and the cement production, and also from the land use change, e.g. by deforestation. The trees are burned or let to rot, whereby the CO_2 storage in the plants is released to the atmosphere. Biomass burning immediately leads to increase of CO_2 concentration in the atmosphere. On the other hand by burning of vegetation the carbon sink is destroyed for a long time.

The inventory of CO_2 the ocean by solution of CO_2, the photosynthesis of terrestrial plants and oceanic phytoplankton represent the main CO_2 sinks. For more details see e.g. [23]. The relative part of the carbon emission remaining in the atmosphere is called Airborne Fraction (AF).

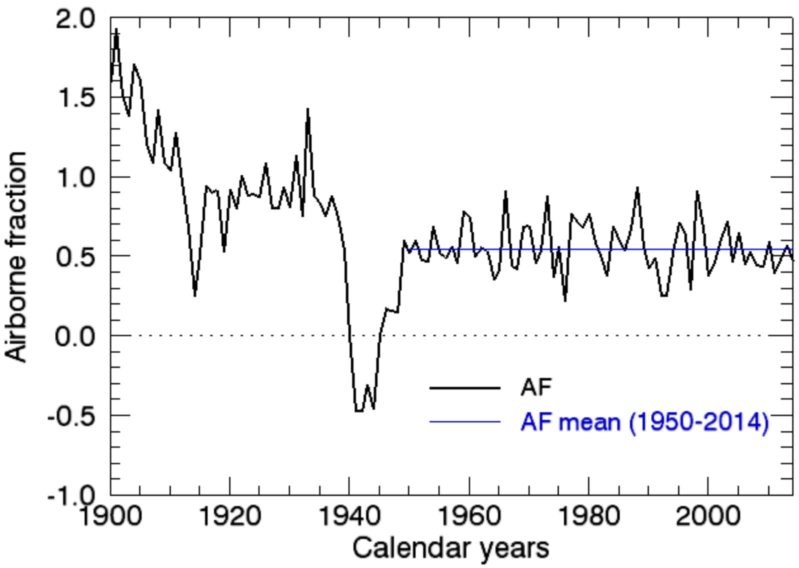

Fig. 3. Airborne fraction related to the CO_2 fuel combustion

The IPCC Fourth Assessment Report (p. 139) [24] follows Keeling [25], who defined the AF in relation to the CO_2 emission taking into account the fossil fuel and cement production. Later the estimation quality of the emission was improved by land use changes and they were included in the CO_2 emissions. Jones et al. [26] have shown that an exponential rise of the CO_2 emissions leads to a constant AF. Here the AF was calculated by the ratio of the first backward differences of the CO_2 and the total CO_2 fuel emission. From 1900 up to 1959 the AF shows variations partially caused by the measurements errors of CO_2 determination from ice cores or by small values of the Carbon emissions. However, strong AF values > 1 indicate that more CO_2 remained in the atmosphere than the amount added by Carbon fuel emission. The total fuel carbon emissions and the carbon emissions by land use are shown in Fig. 4. It is seen that up to about 1910 the emissions by land use are greater than Carbon fuel emission (see also [27]). Negative AF as observed between 1940 and 1945 is caused by a decrease of CO_2 in the atmosphere. At the same time the CO_2 emissions are almost constant. The negative AF or AF values near zero indicate an additional strong CO_2 sink (or they could be caused by higher measurement errors, as well). A significant trend in the AF would indicate a CO_2 feedback (e.g. decrease of the CO_2 ocean uptake). Since the beginning of the direct CO_2 concentration measurements the fraction of the fossil fuel emissions for the time interval up to 2014 shows variations around the mean of 0.55 over the time [24]. The observed here AF seems to be reasonable since 1950 (see Fig. 3). The mean value of the AF is 0.55 ± 0.12. The maximal deviations in 1973, 1988 and 1998 are related to anomaly CO_2 growth rates caused by strong ocean CO_2 uptakes variations [22, 25, 28, and 29]. It was established that the strong El Niño events in 1895–1898, 1911–1916 and 1940–1942 are in coincidence with an increase of the atmospheric CO_2 growth rate. The removal of atmospheric CO_2 by uptake into the ocean is strong, when the Southern oscillation (SO) shifts from its warm phase (El Niño event) to its cool phase (La Niña event) and coincided with a warm to cool phase change of the Pacific Decadal Oscillation (PDO) and with lower temperatures and progressive weakening of the Atlantic thermohaline circulation [20]. The sea-surface warming during El Niño reduced the upwelling of CO_2 rich water which resulted in a reducing of CO_2 outgassing and an enhancement of the CO_2 uptake, respectively [30]. The minimum of the AF in 1992/1993 is related to the Monte Pinatubo eruption and the maximum observed around 2003 is connected to anomalies during the strong heatwave observed in Europe [31].

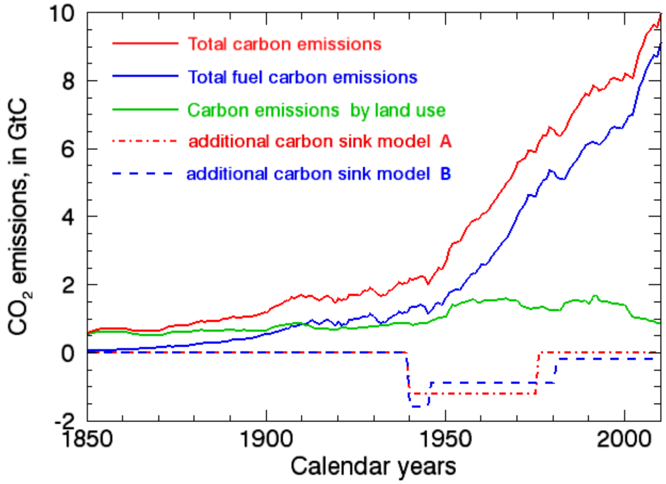

Fig. 4. Global total CO_2 emission by fuel combustion (blue line), the emission by land use changes (green line) and the total CO_2 emissions as the sum of the fuel combustion and land use change (red line). Models for additional carbon sinks (negative values for emissions) are drawn by dashed dotted red line for model A and by dashed blue line for model B.

In contradiction to the argument of strong ocean uptake, Rafelski et al. [27], Truderinger et al. [32] and Rubino et al. [33] concluded, that the plateau in the CO_2 atmospheric concentration after 1940 is likely caused by land air temperature decreasing over the Northern Hemisphere. Bastos et al. [34] have found that cropland abandonment in the Former Soviet Union, as a consequence of the WWII, could explain the CO_2 plateau, due to increase of CO_2 absorption by vegetation recovery and by increase of organic matter in soil.

More detailed studies have shown later that the human part on the additional CO_2 sink by the cropland due abandonment in the Former Soviet Union is about 6–10 % of the gap sink required to explain the plateau [35]. Bastos et al. [35] have outlined that it is likely decreases in agricultural areas during WWII might have also occurred in other regions and could additionally contribute to the sink gap. Such events may not be included in FSU–REF data due to the use of different sources of information as is the case, for example, of China. They claimed that the part of the additional sink of about 60% has a natural source. The reason of the CO_2 stabilization up to now is not fully understood.

The response of the concentration of CO_2 in the atmosphere to changes in the carbon emissions can be estimated in the first order using the concept of the Impulse Response Function (*IRF*) (or Green's function), where CO_2 can be represented by the sum of earlier anthropogenic emissions e at time t' multiplied by the fraction remaining still airborne after time $t-t'$, given by the IRF [36]:

(1) $$CO_2 = c \cdot \int_{t_0}^{t} e(t')IRF(t-t')dt' + CO_2(t_0),$$

where the IRF is given by a sum of exponential functions

$$IRF(t) = a_0 + \sum_{i=1}^{n} a_i \cdot \exp\left(\frac{-t}{\tau_i}\right) \qquad for\ t \geq 0,$$

and a_0 is the part which remains permanently in the atmosphere and a_i are the fractions associated with the time scale τ_i. *IRF* is not an invariant function, but depends on the magnitude of the carbon emissions [37]. If the carbon emissions are given in GtC then the factor *c* is about 0.47 ppmv/GtC to obtain the CO_2 concentration in ppmv. This constant can be used for tuning to achieve the best adjustment. The *IRF* concept was developed for cost effective estimations of the atmospheric CO_2 concentration as response to different future anthropogenic emission scenarios and describes the CO_2 ocean uptake. Biological sources and sinks are not included in the model to obtain the *IRF* [37]. Using *IRF* parameters of the standard Bern SAR model the integration of the CO_2 emissions (see unfccc.int/resource/brazil/carbon.html) gives a result close to the obtained one by

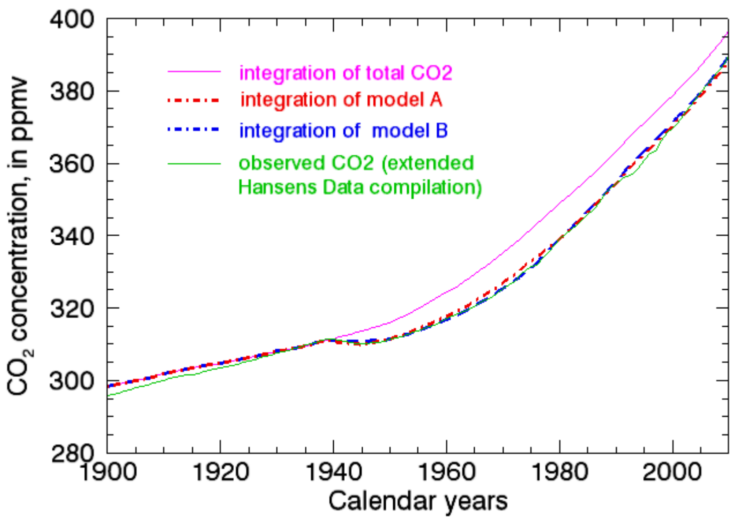

Fig. 5. Results of the integration of the total CO_2 emissions (defined as the sum of the total CO_2 fuel emission and the emission by change of land use) (continuous magenta line), the integration of the total CO_2 emissions reduced by additional sinks model A (dashed dotted red line), and model B (dashed dotted blue line) in comparison with the observed CO_2 concentration (using the extended Hansen's data compilation) (continuous green line)

ice core, firn and atmospheric measurements (as obtained by the extended Hansen's data compilation). By the integration of the original data consisting of the sum of the total fuel emissions and the land use emissions no plateau can be observed (the magenta line in Fig. 5). The slowdown of the emissions during the period between the beginning of the WWI and the end of the WWII lead only to a stabilization of the grow rate from about 0.5 Gt carbon (0.24 ppmv CO_2) per year up to approximately 1.0 Gt carbon (0.47 ppmv CO_2). After this the grow rate fast increase up to 4 Gt carbon (1.9 ppmv CO_2) per year. However if the total carbon fuel and land used emissions during the interval between 1940 and 1975 are reduced yearly by 1.2 Gt carbon (see Fig. 4, sink model A) then the integration results form a plateau very close to the ones obtained by the ice core and firn air CO_2 measurements (the dashed dotted red line in Fig. 5). (The total sink corresponds to about 43 GtC, see Fig. 4). Here of course the precise shape of the function describing the carbon reduction cannot be reconstructed, by reason of the insensitivity of the integration. A very like result for the total CO_2 emissions is formed by a strong carbon reduction of 1.6 Gt carbon per year during 1940–1945 following by a permanent sink of 0.9 Gt carbon per year up to 1980 and after this a sink of 0.2 Gt carbon (see Fig. 4, sink model B), with total carbon sink of about 47 GtC (the dashed dotted blue line in Fig. 5). The goal of this work was not to obtain a good adjustment to the measured atmospheric CO_2. The aim was to demonstrate that the plateau can be observed only, if the carbon reduction takes place suddenly by a sink formed by one longer impulse or by one stronger short impulse followed by a stepwise sequence of weaker impulses. Of course this is true only in the framework of the used model (based on IRF). It has to be mentioned that from the slowdown of CO_2 emissions directly follows an equivalent slowdown of the radiation forcing function [38].

In the following section the influence of the CO_2 concentration observed by measurements on one hand and estimated by the integration of observed total carbon emissions (the sum of the total fuel emissions and the land use emissions) on the other hand, on the temperature is estimated using linear multiple regression model.

Regression model

The long-time global temperature trends are determined by the concentration of the carbon dioxide (CO_2) in the atmosphere. In our regression model the CO_2 data compilation from Hansen is used (http://www.climateaudit.info/data/hansen/giss_ghg.2007.dat). The data, covering the period 1850–2006, were extended to 2016 adding the obtained annual CO_2 by regression of the Hansen data against the CO_2 measurements provided by the Mauna Loa observatory (ftp://ftp.cmdl.noaa.gov/ccg/co2/trends/co2_annmean_mlo.txt).

To study the influence of different factors on climate Werner et al. [39] were used the following linear regression model:

$$(2) \qquad T_{obs} = const + \beta_1 * \ln(CO_2/280\,ppmv) + \beta_2 * AMO + \beta_3 * PDO + \beta_4 * TSI + \\ + \beta_5 * SO + \beta_6 * AOD + \varepsilon,$$

where at the left hand side T_{obs} is the observed annual temperature anomaly and the regressors at the right hand side are the logarithm of CO_2 referred to its pre-industrial value of 280 ppmv, the Total solar irradiances (TSI), and the indices of the AMO, of the Pacific decadal oscillation (PDO), of the Southern oscillation (SO) and of the Aerosol optical depth (AOD).

To avoid collinearity in the regression other greenhouse gases except CO_2 were not included in the regression because the time evolution of their atmospheric concentrations is similar to the one of CO_2. Moreover other radiative active gases as methane (CH_4), halocarbons and nitrous oxide (N_2O) have a higher warming potential per molecule than CO_2, but their amounts in the atmosphere are much smaller. So the climate change is driven mainly by CO_2 [40]. The CO_2 forcing is defined as $\Delta F = 5.35 * \ln(CO_2 / 280ppmv)\, Wm^{-2}$ [40]. In our computations, the used time interval was limited from 1900 up to 2010, because the temperature observations are more accurate since the beginning of 1900 than before and the carbon emissions are available up to 2010. The climate sensitivity can be easily determined by the linear regression equation with the help of the relation $\Delta T = \lambda\, \Delta F$. Werner et al. [39] have shown that the residuals in Eq. 1 can be described by an AR(1) model and the time series size can be replaced by its effective number [41]. By means of the effective sample size the effective standard deviations and the Students' effective t-values were calculated. The temperature sets of the leading climate centres as NOAA and Met Office are close to each other and do not give different results. In view of this, here only one temperature set, namely the HadCRUR4 temperature set of the UK Met Office is used.

In Table 1 the results are summarized including only the statistically significant regressors at the confidence level of 0.95, where the critical t-value is about 1.96. The corresponding to the 1-σ error effective *t*-value, taking into account the residuals autocorrelation, was denoted as t_{eff}. A stepwise regression with backward elimination of the most non-significant term was performed. To estimate the temperature anomalies, two models were applied. In the first model the real atmospheric CO_2 concentration was used as regressor, and an explained variance of 0.926 was achieved. In the second model the total CO_2 emissions obtained from equation 1 were used as regressor, an explained variance of 0.923 was observed. Both models distinguished not significantly one from the other and both statistic models describe the observed temperature anomalies very well.

Table 1. Results of the stepwise regression Eq. 2

note		β_1	β_2	β_4	β_5	R^2
Model 1 Atmospheric CO_2	Regr. coeff. σ $t_{eff.}$	2.734 0.097 22.20	0.488 0.038 10.10	0.058 0.017 2.62	-0.028 0.006 -3.53	0.926
Model 2 Integrated total CO_2 (fuel and Land use)	Regr. coeff. σ $t_{eff.}$	2.483 0.090 22.10	0.533 0.038 10.70	0.040 0.018 1.74	-0.027 0.006 -3.22	0.923

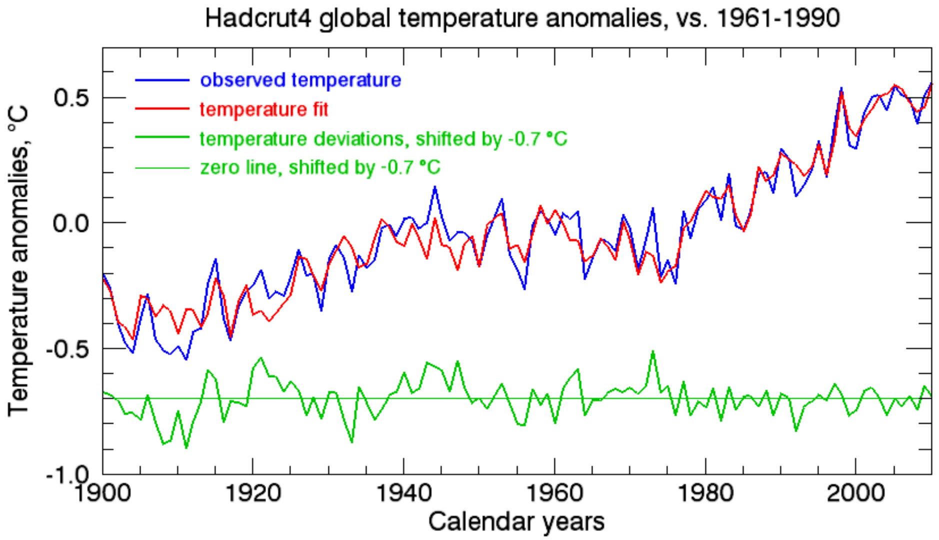

Fig. 6. The global annual temperature anomalies by the HadCRUT4 data set (blue line), the ones by the fitted using the regression equation (2) for model 1 temperatures (red line) and the differences between the observed temperatures and the fitted temperatures (green line). For better eyesight, the deviations were shifted down by 0.7 °C.

The obtained results for the fitted temperature anomalies compared to the observed ones and the computed temperature deviations for model 1 are shown in Fig. 6. (There are shown only the results for model 1, because the results for model 2 are very close to the ones of model 1). It is seen that the cooling and warming periods are very well captured by the model. The long-time trend is determined by the CO_2 term and the AMO influence in both models. These are the main regressors, describing the observed global temperature anomalies. The multiple correlation taking in consideration only these two terms is about 0.951 for model 1 and 0.953

for model 2 with an explained variance of approximately 0.905 and 0.907, respectively. In comparison to the first model in the second one the influence of the CO_2 term is somewhat smaller which is compensated by a stronger impact of the AMO. The temperature change by doubling the CO_2 content would be 1.85 °C, corresponding to a climate sensitivity of 0.5 K/Wm^{-2}, based on equilibrium change in global mean temperature. The temperature influence of TSI is small, about 0.06 °C, when TSI is changed by 1 W/m^2, corresponding to a change of the solar activity from its minimum to its maximum (or vice versa). The SOI influence is also low, but it is more important at regional scales (not shown here). It has to be mentioned, that in a model without CO_2 the high autocorrelation of the residuals leads to a significant influence only of the AMO.

By the regression equations, the adjusted temperature, describing the CO_2 influence on the temperature anomalies, can be easy calculated by removal of the temperature impacts of AMO, TSI and SOI.

Adjusted Temperature estimation

To demonstrate the relationship between the CO_2 concentration and the global temperature anomaly, here, as it was mentioned above, adjusted temperatures were calculated by removal of the influences of AMO, TSI and SOI.

(3) $$T_{adj} = \beta_1 * \ln(CO_2/280\ ppmv) + T_{obs} - T_{fit},$$

where $T_{obs} - T_{fit}$ is equivalent to the residuals ε.

The obtained adjusted temperatures T_{adj} follow very close the time evolution of the CO_2 concentration (see Fig. 7). It has to be pointed out that a climate pause caused by CO_2 after 1998 is not noticeable. If the temperatures would be not influenced by CO_2 and the temperature anomalies increase would be generated only by a linear trend the residuals would show a CO_2 induced signal. The residuals $T_{obs} - T_{fit}$ (which are equal to the differences between the adjusted temperatures and the CO_2 temperature impacts) are very close for both models. The maximal deviations of the difference of the temperature fits of both models are of the order of about 0.04 °C and they are smaller than the non-explained variance of the fits themselves but show clearly a CO_2 induced signal, like the difference of the model CO_2 impacts on the temperatures (see Fig. 7).

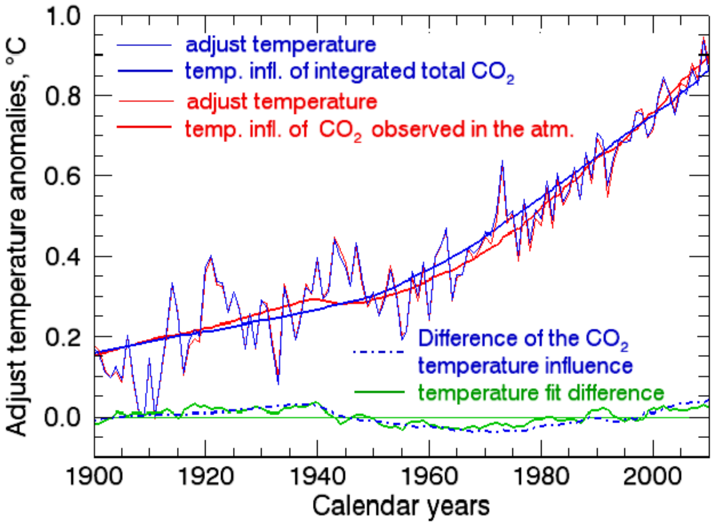

Fig. 7. The adjusted by equation (3) temperatures (thin blue and thin red line) and the CO_2 influence on temperature (thick blue and thick red line) by both regression models (see Table 1). The difference of adjusted temperature fits by the two regression models is presented by a thick green line. The dashed blue line shows the difference of the CO_2 influence on the temperature obtained by the two regression models.

For illustration of the slowdown observed in the CO_2 concentration and temperature anomalies it was assumed, that the world economy gathered the same speed of development as after 1950 immediately after 1939, so the growth rate of CO_2 after 1939 would be the same as after 1950. Then the adjusted temperature T_{adj}^* can be estimated replacing CO_2 by:

$$CO_2^*(t) = CO_2(t - 10) \quad \text{for} \quad t > 1939. \tag{4}$$

Based on the piecewise linear regression investigations of the long-lived radiation factors Estrada et al. [38] have identified a strong breakpoint in the CO_2 radiative forcing about 1960 related to the post-war economic expansion with data sets up to 2010. The authors proposed a radiation forcing of CO_2 without the slowdown (see Supplementary information in [38]) like CO_2 forcing described here. However in [38] temperature changes due to the shifted CO_2 concentrations were not recalculated. Here the results for $T_{adj}(CO_2)$ and $T_{adj}^*(CO_2^*)$ are shown together with the original data in Fig. 8 using the regression model A.

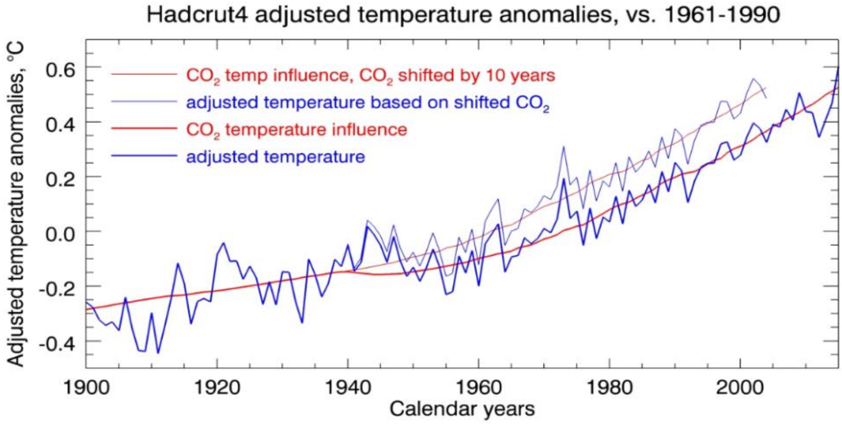

Fig. 8. Adjusted by equation (3) temperature anomalies (thick blue line) and the CO_2 temperature influence (thick red line, regression model 1) and the temperature and the CO_2 term developments assuming that the CO_2 grow rates observed after 1950 would be expected immediately after 1939 (shown by thin lines).

Mainly the additional CO_2 sink lead to a decrease of the CO_2 concentration growth rate, which caused a deceleration of the adjusted temperature anomalies. As a result of the CO_2 slowdown the temperature increase decelerates and it can be speculated that without the CO_2 slowdown the temperature today probably would be approximately 0.15 °C higher. This effect can be clearly seen only in the adjusted temperatures. For the observed temperature anomalies the effect is covered by the other temperature impacts, mainly by the AMO influence.

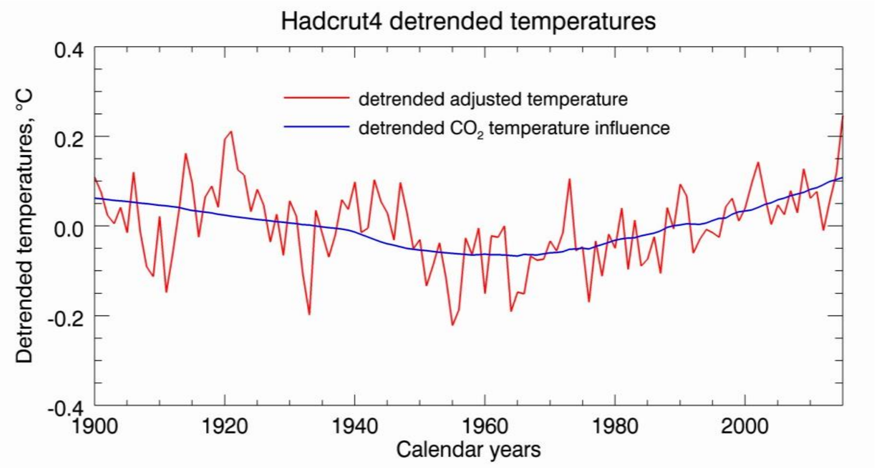

Fig. 9. Time evolution of the linear detrended adjusted temperatures and the linear detrended CO_2 temperature influences (for the regression model 1)

The relation between the adjusted temperature and the CO_2 radiation forcing at shorter time scales determined by the linear detrended series is shown in Fig. 9. It is to be noted again the close connection between the detrended adjusted temperature and the detrended CO_2 term. The close linear relation between the CO_2 temperature influence and the adjusted temperature is outlined also by the scatter plot (Fig. 10). Any deviation from a linear relation cannot be detected. Due to the at least partially man-made CO_2 slowdown and the close relation to the temperature changes at long time and shorter time scales we can conclude that the CO_2 is the leading variable of the relation between the temperature changes and CO_2 after the Pre-industrial Era.

Of course the statistical proof of causality and the proof of the human impact on climate change are complicated [42, 43]. As it is seen in Fig. 1 the residuals are not homoscedastic. The variance in the time interval up to approximately 1975 is evidently greater than after that time and the autocorrelation is also not constant over the whole time interval. The statistic investigations are more complex because the global annual temperature anomalies series have structural breaks. In the case of filtered temperature series generated by removal of the AMO temperature influence the global temperatures have a structural break approximately in 1970, as well [38, 44].

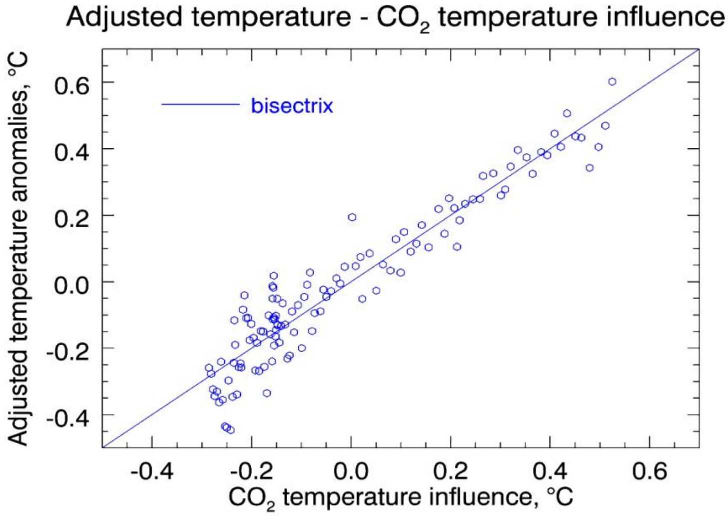

Fig. 10. Scatter plot of the CO_2 temperature influences and the adjusted temperatures

The aim of the present paper is not the statistical proof of the cause-effect relationship. Here the main goal was to demonstrate the evidence of the relation-ship between the CO_2 radiative forcing and the temperature change where the leading variable during the Industrial Era is CO_2.

Summary and conclusions

The rapid economic development after 1950 was accompanied with enormous consumption of oil up to the first oil shock in 1973. Since this time by different economic and politic reasons the growth of the emissions was decelerated. The simultaneous CO_2 ocean uptake shows high variations forced by strong ENSO events. The concentration of the atmospheric CO_2 increases continuously up to now. Due to the man-made effect of the depression of the World economic development during the World War I and after it, the Great Depression and the World War II the CO_2 emission was slowdown. The integration of the total CO_2 emission using the IRF concept shows that the observed slowdown of the CO_2 emission is not sufficient to explain the plateau of the atmospheric CO_2 concentration. To account for the CO_2 plateau one or more additional sinks are necessary, as it was obtained before by solution of the inverse problem and climate models. The AF indicates an additional strong CO_2 sink as well. Here the observed CO_2 content in the atmosphere was obtained by the integration of two different models of additional CO_2 sinks. The results show that the integration is not sensitive to the explicit form of the sinks. Furthermore based on regressions models by subtraction of temperature impacts excluding these of CO_2 adjusted temperatures were determined. It was demonstrated that the adjusted temperature and the detrended adjusted temperature follow very close the course of the radiative CO_2 forcing and the detrended course of the radiative CO_2 forcing, respectively. That means that both the adjusted temperature and the radiative CO_2 forcing have the same long time trend and the same trend at shorter time scales. Moreover a CO_2 signal was found in the adjusted global temperature anomalies and consequently in the global temperatures.

Assuming that the CO_2 grow rates would not decelerate after 1939 and the economy would have the same development as after 1950 the global temperature anomalies would be approximately 0.15 °C higher than the tempera-tures today.

In the used here time interval after the preindustrial era the atmospheric concentration was determined mainly by the energy consumption. It was shown that the CO_2 slowdown observed between 1939 and 1950 was at least partially man-made. Therefore the CO_2 is the leading variable in the relationship with the global temperature change.

The CO_2 slowdown and the deceleration of the temperature increase at the same time visible in the adjusted temperatures can be considered as a fingerprint of the human impact on the climate warming process.

References

1. Lean, J. L., D. H. Rind. How natural and anthropogenic influences alter global and regional surface temperatures: 1889 to 2006, Geophys. Res. Lett., 2008, 35, L18701. doi:10.1029/2008GL034864
2. Forster, G. and S. Rahmstorf. Global temperature evolution 1979–2010, Env. Res. Lett., 2011, 6, 8-xx. http://iopscience.iop.org/article/10.1088/1748-9326/6/4/ 044022/meta
3. Schlesinger, M. E. and N. Ramankutty. An oscillation in the global climate system of period 65-70 years, Nature, 1994, 367, 723–26. doi:10.1038/367723a0
4. Enfield, D. B. and L. Cid-Serrano. Secular and multidecadal warmings in the North Atlantic and their relationships with major hurricane activity, Int. Jour. Climatol., 2010, 30, 2, 174–84. doi:10.1002/joc.1881
5. Wang, C. and S. Dong. Is the basin-wide warming in the North Atlantic Ocean related to atmospheric carbon dioxid and global warming? Geophys. Res. Lett., 2010, 37, L08707. doi:10.1029/2010GL042743
6. Knudsen, F.M., M.-S. Seidenkranz, B. H. Jacobsen et al. Tracking the Atlantic Multidecadal Oscillation through the last 8,000 years, Nature communications, 2011. doi:10.1038/ncomms1186
7. Weng, H. Impacts of multi-scale solar activity on climate. Part II: Dominant timescales in decadal-centennial climate variability, AAS, 2012, 4, 887–908. doi:10.1007/s00376-012-1239-0
8. Knight, J. R., Folland, C. K., and Scaife, A. A. Climate impacts of the Atlantic Multidecadal Oscillation, Geophys. Res. Lett., 2006, 33, L17706. doi:10.1029/2006GL026242
9. Rohde, R., R. A. Muller, R. Jacobsen et al. A New Estimate of the Average Earth Surface Land Temperature Spanning 1753 to 2011, Geoinfor Geostat: An Overview 1:1. doi:10.4172/2327-4581.1000101
10. Zhou, J. and K. K. Tung. Deducing multidecadal anthropogenic global warming trends using multiple regression analysis, J. Atmos. Sci., 2013, 70, 1, 3–8. doi:10.1175/JAS-D-12-0208.1
11. Ballantyne A. P, C. B. Alden, J. B. Miller, P. P. Tans, and J. W. White. Increase in observed net carbon dioxide uptake by land and oceans during the past 50 years, Nature, 2012, 488, 7409, 70-2. doi:10.1038/nature11299
12. Jones G. S., S. F. B. Tett , and P. A. Stott. Causes of atmospheric temperature change 1960–2000: A combined attribution analysis, Geophys. Res. Lett., 2003, 30, 5, 1228. doi:10.1029/2002GL016377
13. Braganza, K., D. J. Karoly, and J. M. Arblaster. Diurnal temperature range as an index of global climate change during the twentieth century, Geophys. Res. Let., 2004, 31, L13217. doi:10.1029/2004GL019998
14. Alexander, L. V., X. Zhang, T. C. Peterson et al. Global observed changes in daily climate extremes of temperature and precipitation, J. Geophys. Res., 2006, 1, 111. doi:10.1029/2005JD006290
15. Siegenthaler, U. and F. Joos. Use of a simple model for studying oceanic tracer distribution and the global carbon cycle, Tellus, 1992, 44B, 186–207.

16. Siegenthaler, U. and H. Oeschger. Biospheric CO_2 emissions during the past 200 years reconstructed by deconvolution of ice core data, Tellus, 1987, 39B, 140–54. doi:10.1111/j.1600-0889.1987.tb00278.x
17. Houghton, R. A., Balancing the global carbon budget, Ann. Rev. Earth Planet. Sci., 2007, 35, 313–47.
18. Friedrich, J. and T. Damassa. The History of Carbon Dioxide Emissions, 2014. http://www.wri.org/blog/ 2014/05/history-carbon-dioxide-emissions
19. Hansen, J., M. Sato. Greenhouse gas growth rates. PNAS, 2004, 101, 46, 16109–114. http://www.pnas.org/content/suppl/2004/11/02/0406982101.DC1/06982 SupportingText.html
20. MacFarling Meure, C., D. Etheridge, C. Trudinger et al. The Law Dome CO_2, CH_4 and N_2O Ice Core Records Extended to 2000 years BP, Geophys. Res. Lett., 2006, 14, L14810. doi:10.1029/2006GL026152
21. Langenfelds, R. L., L. P. Steele, M. V. Van der Schoot et al. Atmospheric methane, carbon dioxide, hydrogen, carbon monoxide and nitrous oxide from Cape Grim flask air samples analysed by gas chromatography. In: Baseline Atmospheric Program Australia. 2001–2002, ed. J.M. Cainey, N. Derek, and P.B. Krummel (editors), Melbourne: Bureau of Meteorology and CSIRO Atmos. Res., 2004, 46–47.
22. Etheridge, D. M., L. P. Steele, R. L. Langenfelds, R. J. Francey, J.-M. Barnola, and V. I. Morgan. Natural and anthropogenic changes in atmospheric CO_2 over the last 1000 years from air in Antarctic ice and firn, J. Geophys. Res., 1996, 4115–28. doi:10.1029/95JD03410
23. Heinze, C., S. Meyer, and N. Goris. The ocean carbon sink – impacts, vulnerabilities and challenges, Earth Syst. Dynam., 2015, 6, 3R.L.27–358. doi:10.5194/esd-6-327-2015
24. AR4 Climate Change 2007: The Physical Science Basis. Contribution of Working Group I to the Fourth Assessment Report of the Intergovernmental Panel on Climate Change [Solomon, S., D. Qin, M. Manning, Z. Chen, M. Marquis, K.B. Averyt, M. Tignor and H.L. Miller (eds.)]. Cambridge University Press, Cambridge, United Kingdom and New York, NY, USA, 2007, 996 pp. on p. 139.
25. Keeling, C. D., T. P. Whorf, M. Wahlen, and J. v. D. Pflicht. Interannual extremes in the rate of atmospheric carbon dioxide since 1980, Nature, 1995, 375, 666–70. doi:10.1038/375666a0
26. Jones, C. D, P. M. Cox, and C. Huntingford. The atmospheric CO_2 airborne fraction and carbon cycle feedbacks, 2007. https://www.esrl.noaa.gov/gmd/co2conference/posters_pdf/jones1_poster.pdf
27. Rafelski, L. E., S. C. Piper, and R. F. Keeling. Climate effects on atmospheric carbon dioxide over the last century, Tellus B, 2009, 61, 5, 718–31. doi:10.1111/j.1600-0889.2009.00439.x
28. Joos, F., R. Meyer, M. Bruno, M. Leuenberger. The variability in the carbon sinks as reconstructed for the last 1000 years, Geophys. Res. Let., 1999, 26, 10, 1437–40. doi:10.1029/1999gl900250
29. Francey, R. J., P. P. Trans, C. E. Allison, I. G. Enting, J. W. C. White, and M. Troller. Changes in oceanic and terrestrial carbon uptake since 1982, Nature, 1995, 373, 326–30. doi:10.1038/373326a0

30. Ishii, M., H. Y. Inoue, and T. Midorikawa. Spatial variability and decadal trend of the oceanic CO_2 in the western equatorial Pacific warm/fresh water, Deep-Sea Res. Pt. II, 2009, 56, 591–606, doi:10.1016/j.dsr2.2009.01.002
31. Jones, C. D. and M. P. Cox. On the significance of atmospheric CO_2 growth rate anomalies in 2002–2003, Geophys. Res. Lett., 2005, 632, L14816. doi:10.1029/2005GL023027
32. Truderinger, C. M., I. G. Enting, P. J. Rayner, R. J. Francey. Kalman filter analysis of ice core data 2. Double deconvolution of CO_2 and $\delta^{13}C$ measurements, J. Geophys. Res., 2002, 107, D20, 4423. doi:10.1029/2001JD001112
33. Rubino, M., D. M. Etheridge, C. M. Trudinger et al. A revised 1000 year atmospheric $\delta^{13}C$-CO_2 record from Law Dome and South Pole, Antarctica, J. Geophys. Res.: Atmosphere, 2013, 118, 8482–99. doi:10.1002/jgrd.50668
34. Bastos, A., P. Ciais. J. Barichivich et al. Re-evaluatingthe1940s CO_2 plateau, Biogeosciences, 2016, 13, 4877–97. doi:10.5194/bg-13-4877-2016
35. Bastos, A., A. Peregon. É. A. Gani et al. The contribution of land-use change versus climate variability to the 1940s CO_2 plateau: Former Soviet Union as a test case, Biogeosciences Discuss., doi:10.5194/bg-2017-26
36. Joos, F., R. Roth, J. S. Fuglestvedt et al. Carbon dioxide and climate impulse response functions for the computation of greenhouse gas metrics: a multi-model analysis, Atmos. Chem. Phys., 2013, 13, 2793–2825. doi:10.5194/acp-13-2793-2013
37. Maier-Reimer, E. and K. Hasselmann. Transport and storage of CO2 in the ocean - an inorganic ocean-circulation carbon cycle model, Climate Dynamics, 1987, 2, 2, 63–90. doi:10.1007/BF01054491
38. Estrada, F., P. Perron, and B. Martínez-López. Statistically derived contributions of diverse human influences to twentieth-century temperature changes, nature geoscience, Advanced online publication, Supplementary information, 2013. doi:10.1038/NGEO1999
39. Werner R., D. Valev, D. Danov, V. Guineva, and A. Kirillov. Analysis of global and hemispheric temperature records and prognosis, Adv. Space Res., 2015, 55, 12), 2961–973. doi:10.1016/j.asr.2015.03.005
40. Myhre, G., E. J. Highwood, K. P. Shine, and F. Stordal. New estimates of radiative forcing due to well mixed greenhouse gases, Geophys. Res. Lett., 1998, 25, 2715–2818. doi:10.1029/98GL01908
41. Thiébaux, H. J. and F. W. Zwiers. The Interpretation and Estimation of Effective Sample Size, Journal of Appl. Meteor, 1984, 5, 800–11. doi:10.1175/1520-0450(1984)023<0800:TIAEOE>2.0.CO;2
42. Stern, D. I. and R. K. Kaufmann. Detecting a global warming signal in hemispheric temperatures series: A structural time series analysis, Climatic Change, 2000, 47, 411–38. doi:10.1023/ A:1005672231474
43. Kaufmann, R. K. and D. I. Stern. Cointegration analysis of hemispheric temperature relations, J. Geophys. Res., 2002, 107, D2, 4012. doi:10.1029/2000JD000174
44. Werner R., D. Valev, D. Danov, and V. Guineva. Study of structural break points in global and hemispheric temperature series by piecewise regression, Adv. Space Res., 2015, 56, 11, 2323-34. doi:10.1016/j.asr.2015.09.007

ГЛОБАЛНИ ТЕМПЕРАТУРНИ АНОМАЛИИ, СВЪРЗАНИ СЪС СПАД НА КОНЦЕНТРАЦИЯТА НА CO_2 В АТМОСФЕРАТА, ОТ 1939 Г. ДО 1949 Г.

Р. Вернер, В. Гинева

Резюме

Известно е, че въглеродният диоксид (CO_2), акумулиран в атмосферата, е главният драйвер на климата. Първите точни непрекъснати преки измервания на концентрацията на атмосферния CO_2 са проведени от Keeling от 1958 г. в обсерваторията Mauna Loa. Измерванията продължават до днес. Сондирането на ледения слой в Low Dom започва през 1969 г. с програмата ANAPE.

Интегрирането на тоталната емисия на CO_2 с помощта на импулсна апаратна функция показва, че наблюдаваният спад на емисията на CO_2 не е достатъчен, за да обясни полученото плато и е необходимо да се включат допълнителни потоци. На основата на мулти-регресионни модели бяха определени изчистените „напаснати" глобални температури чрез изключване на други температурни влияния, освен свързаните със CO_2.

Изчистените „напаснати" температури на хода на радиацията на CO_2, разликата между времевото развитие на оценените уточнени температури със спада на CO_2 и без него, а също и кратковременните трендове показват много ясно тясната връзка между температурната промяна и парниковия ефект от CO_2. Показано е, че спадът на емисията на CO_2 в периода от 1939 г. до 1950 г. и свързаната с нея концентрация на CO_2 в атмосферата, породена поне отчасти от човешката дейност, предизвиква по-бавно нарастване на температурните аномалии през този период. Следователно CO_2 е водещата променлива в зависимостта: температура на повърхността – CO_2.